RSC Advances

PAPER

Cite this: *RSC Adv.*, 2020, **10**, 35214

Thermal properties and surface chemistry of cotton varieties mineralized with calcium carbonate polymorphs by cyclic dipping

Sunghyun Nam, *[a] Yaewon Park,†[b] Matthew B. Hillyer, [a] Rebecca J. Hron,[a] Nicholas Ernst,[ac] SeChin Chang,[a] Brian D. Condon,[a] Doug J. Hinchliffe,[a] Ericka Ford [b] and Bruce C. Gibb [c]

In this study, hydroentangled cotton nonwovens were identified as effective hosts for mineralization of calcium carbonate ($CaCO_3$) polymorphs to modify and improve their properties. All cotton varieties studied, including raw white cotton, scoured white cotton, and raw brown cotton, readily crystallized $CaCO_3$ *via* a simple cyclic dipping process. A combination of analyses agreed that the surface chemistry of cotton fibers influenced the formation of different $CaCO_3$ polymorphs. Scoured white cotton that consisted of almost pure cellulose predominantly produced the most stable calcite, whereas raw white and raw brown cottons that contain proteins facilitated the production of partial metastable vaterite. The morphology of calcite was better defined on the scoured cotton. The mineralization altered the hydrophobic surface of raw cottons to be hydrophilic, *i.e.*, two-fold increase in moisture regain and decrease in water contact angle from 130 to 0 degrees. The mineralized cottons also exhibited improved thermal resistance, *i.e.*, slower thermal decomposition with decreased activation energies and reduction in heat release capacity by up to 40%.

Received 18th July 2020
Accepted 13th September 2020

DOI: 10.1039/d0ra06265k

rsc.li/rsc-advances

1. Introduction

Calcium carbonate ($CaCO_3$), which is one of the most abundant minerals on Earth making up more than 4% of the Earth's crust, is produced by many living organisms such as in teeth, bones, the shells of mollusks, and skeletons of reefs.[1,2] In their biotic syntheses, the chemistry and structure of organic macromolecules have key roles in the development of mineral phases, *i.e.*, control over polymorphism, crystallographic orientation, and crystal organization.[3] By learning how nature does chemical synthesis, there have been advances in the mineralization on polymeric materials as host templates to impart advantageous properties. The synthetic techniques developed include hydrothermal mineralization[4,5] and cyclical dipping of materials into precursor solutions.[6] Mimicking natural methods of mineralization, the hydrothermal procedure involves the prolonged exposure of the host material to a precursor solution. The host materials that were successfully mineralized with $CaCO_3$ include chitosan/poly(vinyl alcohol)[7] and poly(3-hydroxybutyrate-*co*-3-hydroxyvalerate) nanofibers.[8] Their mineralization, which was initiated at the electron-rich sites of hydroxyl groups and ether linkages of the fibers, took place over about 5–6 weeks. Recent reports demonstrated that the cyclical dipping method at an ambient temperature is efficient for a short period of time. Simply alternating the immersion of nanofibers or membranes in aqueous solutions of calcium chloride ($CaCl_2$) and sodium carbonate (Na_2CO_3) for about 10 cycles deposited $CaCO_3$ minerals throughout the substrates.[9–11]

$CaCO_3$ mineralization occurs as different forms of crystals. Three polymorphs—rhombohedral calcite, orthorhombic aragonite, and hexagonal vaterite—are available. At ambient temperature and atmospheric pressure, calcite is thermodynamically the most stable, followed by aragonite and vaterite. The least stable vaterite is easily transformed into one of the stable phases under appropriate conditions. Although calcite is most stable, a mixture of polymorphs is frequently formed. The size and aggregation state of crystals are also diverse between different syntheses. As the polymorphism of $CaCO_3$ directs the physicochemical properties of mineralization in its application (*i.e.*, adsorbent, filters, and composites), there have been efforts to understand how synthetic variables affect the formation of polymorphs. For example, aragonite, which has a greater refractive index than the other polymorphs, exerts higher performance properties as

[a]*United States Department of Agriculture, Agricultural Research Service, Southern Regional Research Center, 1100 Robert E. Lee Boulevard, New Orleans, LA 70124, USA. E-mail: sunghyun.nam@ars.usda.gov; Tel: +1 504 286 4229; +1 504 286 4390*

[b]*Department of Textile Engineering, Chemistry and Science, The Nonwovens Institute, North Carolina State University, 1020 Main Campus Drive, Raleigh, NC 27606, USA*

[c]*Department of Chemistry, Tulane University, 6823 St. Charles Avenue, New Orleans, LA 70118, USA*

† The present address of Y. Park is the Advanced Science Research Center, The Graduate School and University Center of the City University of New York (CUNY), New York, NY 10016, USA. The USDA is an equal opportunity provider and employer.

a filler in paper.[12,13] The nucleation of aragonite was found to be facilitated by manipulating reaction conditions such as high pH,[14] presence of magnesium ions,[15] supersaturation of reactants (Ca^{2+} and CO_3^{2-} ions),[16] and increased temperature.[15] The fraction of polymorphs was also dependent on the construction of host materials. In the mineralization of poly(vinylidene fluoride)/poly(acrylic acid) blend membranes, a mixture of calcite and vaterite was formed; however, vaterite was more populated inside the membrane than on the membrane surface.[10] For poly(vinyl alcohol) nanofibers, seeding surfmers in their electrospinning, which had formed polymerized micelles, modified the crystal growth into partial vaterite phases.[11] The vaterite phases are efficient in adsorbent applications, *i.e.*, formaldehyde adsorbent.[17] These studies suggest that there exist conditions, in which the metastable phase is stabilized, preventing its transformation into the stable polymorphs.

In this study, the mineralization of $CaCO_3$ polymorphs on hydroentangled cotton nonwovens was conducted *via* a cyclic dipping process. This method took advantage of a simple inorganic reaction between Ca^{2+} and CO_3^{2-} on the fiber surface. The formation of $CaCO_3$ polymorphs was examined for different cotton varieties, *i.e.*, raw (white) cotton, scoured (white) cotton, and (raw) brown cotton. Raw white cotton fiber after ginning and mechanical cleaning is composed of 95% cellulose and 5% non-cellulosic components, including proteins, waxes, and pectin.[18] The non-cellulosic components are principally located on the outer layers of the fiber (cuticle and the primary cell wall) and are almost all removed by scouring. As opposed to white cotton, brown cotton has an additional component of condensed tannins, which are responsible for the brown color.[19,20] Such various surface chemistry of cotton fibers was expected to influence the mineralization of $CaCO_3$. A variety of techniques including X-ray diffraction (XRD), Raman spectroscopy, attenuated total reflectance-Fourier transform infrared (ATR-FTIR) spectroscopy, scanning electron microscopy (SEM), and energy-dispersive X-ray spectroscopy (EDS) were used to identify the polymorphs, morphological features, and aggregation of $CaCO_3$ crystals. The altered or improved properties of mineralized cotton nonwoven fabrics—thermal resistance and water/moisture absorbance—were analyzed and discussed.

2. Experimental

2.1. Materials

Mechanically pre-cleaned raw white cotton fiber was obtained from T. J. Beall, Greenwood, MI, USA. Brown cotton was grown at the Southern Regional Research Center, USDA-ARS, New Orleans, LA, USA. Calcium chloride ($CaCl_2$), sodium carbonate (Na_2CO_3), calcium carbonate ($CaCO_3$), Triton X-100, and acetic acid were purchased from Sigma-Aldrich. Sodium hydroxide (NaOH) was purchased from J. T. Baker. All chemicals were used as received. Deionized water was used as a solvent.

2.2. Sample preparation

Hydroentangled nonwoven cotton fabrics were fabricated in the nonwoven pilot plant at the Southern Regional Research Center. The details of nonwoven fabrication using pilot-scale equipment have been described in the literature.[21] The area densities of raw white and raw brown nonwoven fabrics were measured according to ASTM D 6242-98 and were 55 ± 3 g m^{-2} and 127 ± 4 g m^{-2}, respectively. Alkaline scouring of raw white cotton fabrics was carried out according to published procedure.[22] The resulting raw white cotton, scoured white cotton, and raw brown cotton nonwoven fabrics were denoted as raw, scoured, and brown, respectively. The $CaCO_3$ mineralization of cotton fabrics was conducted hydrothermally at room temperature following a previously published method.[11] The cyclic dipping method for cotton mineralization was performed in four steps. A nonwoven fabric (5×5 cm) was (1) dipped in 100 mM aqueous $CaCl_2$ for 30 s; (2) rinsed with water for 30 s; (3) dipped in a 100 mM aqueous Na_2CO_3 solution for 30 s; and (4) rinsed with water again. This four-step cycle was repeated 10 times and air-dried at room temperature (22 ± 1 °C). The obtained mineralized fabrics were denoted as m-Raw, m-Scoured, and m-Brown. The growth of $CaCO_3$ was quantified in terms of the mineralization degree (MD):

$$\mathrm{MD}(\%) = \frac{W_\mathrm{m} - W_\mathrm{o}}{W_\mathrm{o}} \times 100 \quad (1)$$

where W_m and W_o are the dry masses of mineralized and control cotton fabrics, respectively. Three measurements were conducted. The MD values for m-Raw, m-Scoured, and m-Brown were 33, 35, and 26%, respectively.

2.3. Characterization

2.3.1. $CaCO_3$ polymorphs. XRD patterns were obtained using an Empyrean X-ray diffractometer (Malvern Panalytical) using Cu Kα radiation (1.54056 Å). The generator was operated at 45 kV with a beam current of 40 mA. Angular scanning was conducted in the range of $2\theta = 5$–$60°$ at a step size of 0.013° using a PIXcel3D detector. No background correction was made.

Raman spectra were measured using a DXR2 Raman microscope (Thermo Scientific) at the following instrument settings: a 780 nm laser with output power of 5 mW, a 10× confocal microscope objective with 3 μm spot diameter, 5 cm^{-1} spectral resolution, and a 50 μm slit width for 2 s integration time. Three measurements at separate locations were conducted over the spectral range of 250–2000 cm^{-1}.

ATR-FTIR spectra were collected using a Vertex 70v FTIR spectrometer (Bruker Daltonics) equipped with a MIRacle ATR accessory (Pike Technologies) that incorporated a diamond crystal plate as the reflector. Six measurements at different locations for each sample were conducted over the spectral range of 4000–600 cm^{-1} at 4 cm^{-1} resolution and with 32 scans.

The surface morphology and surface composition of mineralized cotton fabrics were examined using field-emission scanning electron microscopy (Quanta 3D FEG FIB/SEM, FEI) equipped with EDX (Apollo XL, EDAX). The samples were coated with platinum using a vacuum sputter coater and observed with an acceleration voltage of 5 keV and a beam current of 13 pA.

2.3.2. Thermal properties. Thermogravimetric (TG) and differential thermogravimetric (DTG) analyses were carried out

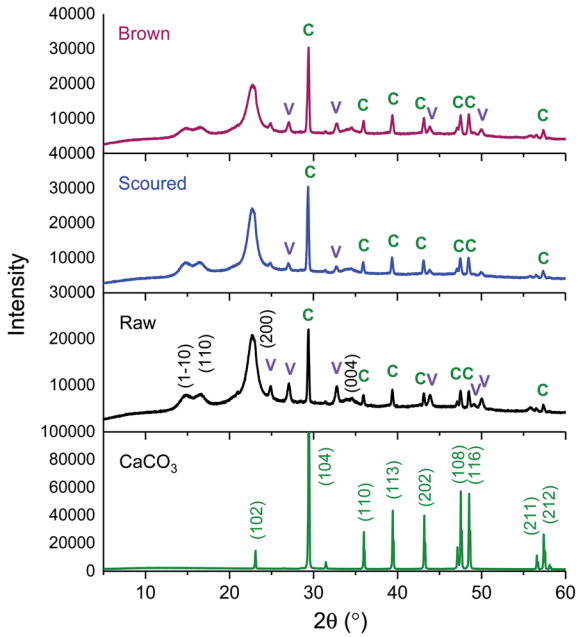

Fig. 1 XRD patterns of mineralized raw, scoured, and brown cotton nonwoven fabrics. The diffraction pattern of reagent-grade $CaCO_3$ powder was presented as comparison. Letters of C and V denote diffraction peaks assigned to calcite and vaterite, respectively.

using a TGA Q500 thermal gravimetric analyzer (TA Instruments) under a nitrogen atmosphere. The nitrogen flow into the furnace was maintained at a rate of 90 mL min^{-1}. Approximately 4 mg of the sample placed in a platinum pan was heated from 30 ± 5 °C to 900 °C with a heating rate of 10 °C min^{-1}. TG and DTG thermograms were analyzed using Universal Analysis 2000 software (TA Instruments). Three measurements were performed.

A thermal kinetics study was conducted using four heating rates of 1, 2, 5, and 10 °C min^{-1} to measure the activation energy (E_a) for the thermal decomposition. The E_a was determined by the isoconversional differential Friedman method[23] using AKTS-Thermokinetics software (version 4.46). This method is based on fundamental kinetic equation (eqn (2)), which describes the rate of conversion, $d\alpha/dt$, as a function of two time-dependent variables—temperature (T) and the conversion of reaction (α). The value of α varies from 0 to 1 from initiation to completion.

$$\frac{d\alpha}{dt} = k(T)f(\alpha) \quad (2)$$

where t is the time, $k(T)$ is the temperature-dependent rate constant, and $f(\alpha)$ is the reaction model associated with the actual reaction mechanism. In this study, $\alpha(t)$ is defined as:

$$\alpha(t) = \frac{\int_{t_0}^{t}(S(t) - B(t))dt}{\int_{t_0}^{t_{end}}(S(t) - B(t))dt} \quad (3)$$

where $S(t)$ and $B(t)$ are the baseline and differential signals, respectively, as a function of t in the TG analysis, and t_0 and t_{end} are the times of initiation and completion of the reaction,

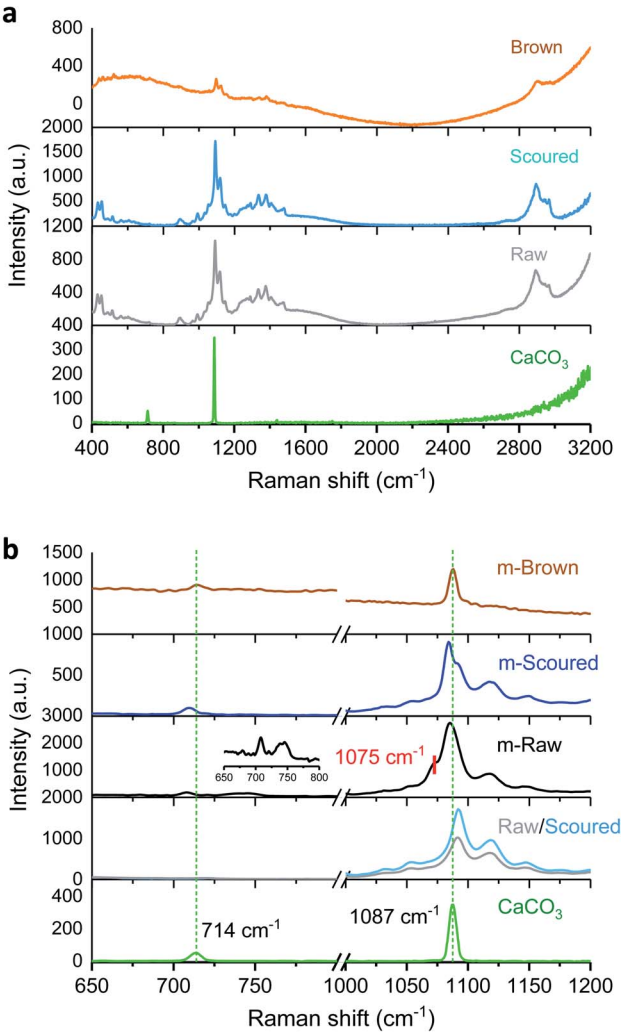

Fig. 2 Raman spectra of raw, scoured, and brown cotton nonwoven fabrics (a) before and (b) after mineralization. The spectrum of reagent-grade $CaCO_3$ was presented as comparison. The inset of (b) shows a magnified spectrum of mineralized raw cotton (m-Raw) at low wavenumbers.

respectively. The $k(T)$ is generally given by the Arrhenius equation:

$$k(T) = A(\alpha)\exp\left(-\frac{E_a(\alpha)}{RT(t)}\right) \quad (4)$$

where $A(\alpha)$ is the pre-exponential factor (min^{-1}), E_a is the activation energy (kJ mol^{-1}), T is the absolute temperature (K), and R is the gas constant (8.314 J K^{-1} mol^{-1}). Substituting eqn (4) into eqn (2) yields:

$$\frac{d\alpha}{dt} = A(\alpha)\exp\left(-\frac{E_a(\alpha)}{RT(t)}\right)f(\alpha) \quad (5)$$

Applying the logarithm to both sides of eqn (5) yields the following equation, which expresses $d\alpha/dt$ as a function of the reciprocal temperature at any α:

$$\ln\left(\frac{d\alpha}{dt}\right) = \ln(A(\alpha)f(\alpha)) - \frac{E_a(\alpha)}{R}\frac{1}{T(t)} \quad (6)$$

Plotting $\ln(d\alpha/dt)$ as a function of $1/T(t)$ at a given α leads to a straight line. The E_a can be calculated from the slope of the straight line $(-E_a(\alpha)/R)$.

Combustion properties were evaluated using a microscale combustion calorimeter (MCC) (MCC-2, Deatak) according to ASTM D 7309-13. Approximately 4 mg of the sample was placed in a ceramic cup and weighed on an analytical balance (XP205, Mettler-Toledo). The sample was then heated to 650 °C at a heating rate of 1 °C s^{-1} in a stream of nitrogen flowing at 80 cm^3 min^{-1}. The volatile thermal decomposition products formed in a pyrolyzer were swept by the gas stream of nitrogen and fully mixed with an oxygen stream at 20 cm^3 min^{-1} in a combustor, where the decomposed products were completely oxidized at 900 °C for 10 s. The oxygen depletion involved in the combustion was determined by the oxygen concentration and flow rate of the combustion gases to measure a heat release rate (HRR). The parameters obtained by the MCC Curve Fit v.2 software (Deatak) are as follows: the specific HRR (W g^{-1}) obtained by dividing the HRR by the initial sample mass; the peak heat release rate (PHRR, W g^{-1}), which is the maximum specific HRR; temperature at PHRR (T_{PHRR}, °C); the heat release capacity (HRC, J g^{-1} K^{-1}) obtained by dividing PHRR by the heating rate; the total heat release (THR, J g^{-1}), which is the area under the specific HRR peak; and char content determined by weighing the sample before and after pyrolysis. An average value of three measurements was presented.

2.3.3. Water/moisture absorption. The contact angle of a water droplet on the fabric was measured using a contact angle analysis equipment (VCA Optima XE, AST Products, Inc.). A 1 μL drop of distilled water was syringed onto the fabric. The image of the droplet on the fabric surface was captured and analyzed to measure contact angles. Contact angles on five different areas were measured, and their average value was presented. The spread behavior of the spotted droplet on the fabric as a function of time were examined using the dynamic contact angle analysis.

The moisture regain of cotton fabrics was measured using a climatic chamber (1722 CS, Mesdan). About 0.5 g of fabric, which had been preconditioned at 23 ± 1 °C and 40 ± 5% relative humidity (RH) for more than 24 h, was weighed. The fabric in a weighing bottle was then placed in the climatic chamber, which had been set at 40 ± 0.5 °C and 90 ± 3% RH, and conditioned for a desired time. After cooling the sample in the weighing bottle to 23 ± 1 °C, the percentage weight gain based on the initial weight of the fabric was measured. Four measurements were conducted for each sample.

3. Results and discussion

3.1. $CaCO_3$ mineralization

The mineralization of $CaCO_3$ polymorphs was examined using a variety of techniques. Fig. 1 shows the XRD patterns of mineralized raw, scoured, and brown cotton nonwoven fabrics as well as reagent-grade $CaCO_3$ powder. The reagent-grade $CaCO_3$ powder exhibited peaks at 23.0°, 29.4°, 36.0°, 39.4°, 43.2°, 47.5°, 48.6°, 56.6°, and 57.4° corresponding to (102), (104), (110), (113), (202), (108), (116), (211), and (212) lattice planes of the pure phase of calcite.[24] For mineralized cottons, four peaks appearing at 14.7°, 16.6°, 22.7°, and 34.8° were assigned to the (1−10), (110), (200), and (004) crystal planes of cellulose Iβ. All mineralized cottons exhibited the well-defined diffraction pattern of calcite that matched with that of reagent-grade $CaCO_3$. They also showed additional peaks at 24.9°, 27.1°, 32.7°, 43.8°, 49.1°, and 50.1°, which represent the (110), (112), (114), (300), (304), and (118) crystal planes of vaterite.[24] This result indicates that cotton varieties studied produced a mixture of calcite and vaterite polymorphs. It is noticeable that the peak intensities of these polymorphs were dependent on cotton variety. The intensity of calcite was higher for the scoured cotton than for raw and brown cottons. Based on the relationship between the peak intensities for the characteristic phases and the abundance of the two polymorphs,

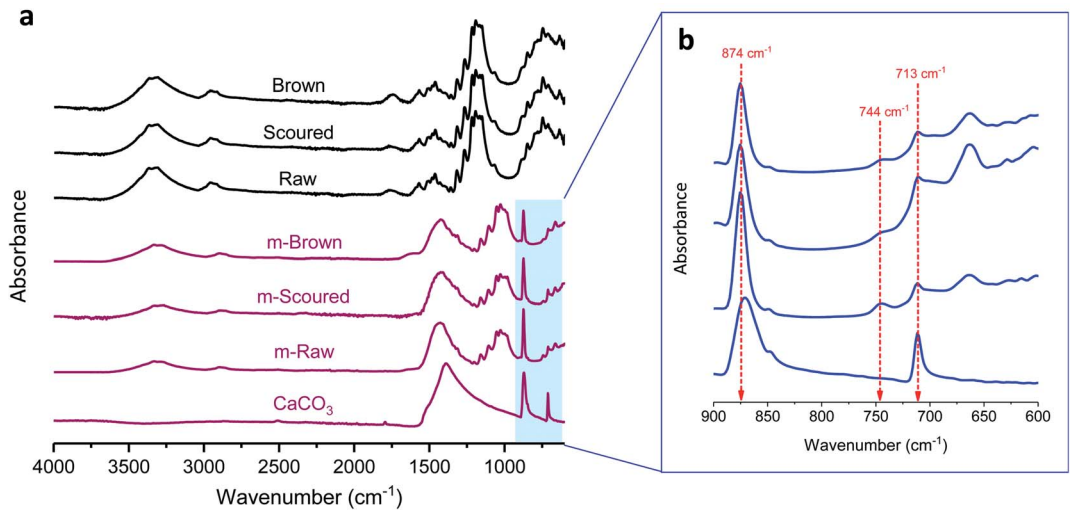

Fig. 3 (a) ATR-FTIR spectra of raw, scoured, and brown cotton nonwoven fabrics before and after mineralization. (b) Close-up of the spectra for mineralized cottons and reagent-grade $CaCO_3$ in the range of 900–600 cm^{-1}.

a percentage fraction of calcite (X_C) was calculated, as described in eqn (7).[25]

$$X_C = \frac{I_{104(C)}}{I_{104(C)} + I_{110(V)} + I_{112(V)} + I_{114(V)}} \quad (7)$$

where I is the intensity, suffixes are Miller indices (hkl), and C and V denote calcite and vaterite, respectively. The calculated X_C values for raw, scoured, and brown cottons were 42.3%, 92.4%, and 53.1%, respectively.

Fig. 2a shows the Raman spectra of control raw, scoured, and brown cotton fabrics as well as reagent-grade $CaCO_3$ powder. The Raman spectra of raw and scoured cottons were similar. Since O–H bonds are weakly polarizable in Raman, O–H vibrations of cotton cellulose are less distinct. The characteristic bands of cotton include δ (CH_2) scissors at 1478 cm^{-1}, δ (CCO) ring deformation at 432 and 453 cm^{-1}, ν (COC) glycosidic link at 1092 and 1118 cm^{-1}, δ (CH_2) wagging and δ (OH) at 1335 cm^{-1}, δ (CH_2) at 1378 cm^{-1}, and ν (CH_2) at 2896 cm^{-1}.[26] Unlike white cotton, brown cotton exhibited a swamped Raman spectrum. The peaks from ν (COC) and ν (CH_2) weakly appeared above the broad line. Previous studies[27–29] reported that brown cotton has additional aromatic carbon components such as condensed tannins, which are known to be a source of brown color.[19,20,30] These complex amorphous polyphenol compounds may be responsible for the broadness of the Raman spectrum. Fig. 2b shows the Raman spectra of mineralized cottons (m-Raw, m-Scoured, and m-Brown) and reagent-grade $CaCO_3$ powder. The $CaCO_3$ powder exhibited the vibration modes at 714 and 1087 cm^{-1}, which are attributed to in-plane bending and symmetric stretching of calcite, respectively.[31–33] The m-Raw cotton exhibited a shoulder peak at around 1075 cm^{-1}, which was assigned to the vibration mode of vaterite.[34] The formation of vaterite was also signified by the appearance a doublet at 738 and 746 cm^{-1} in the magnified spectrum at low wavenumbers (inset of Fig. 2b).[34]

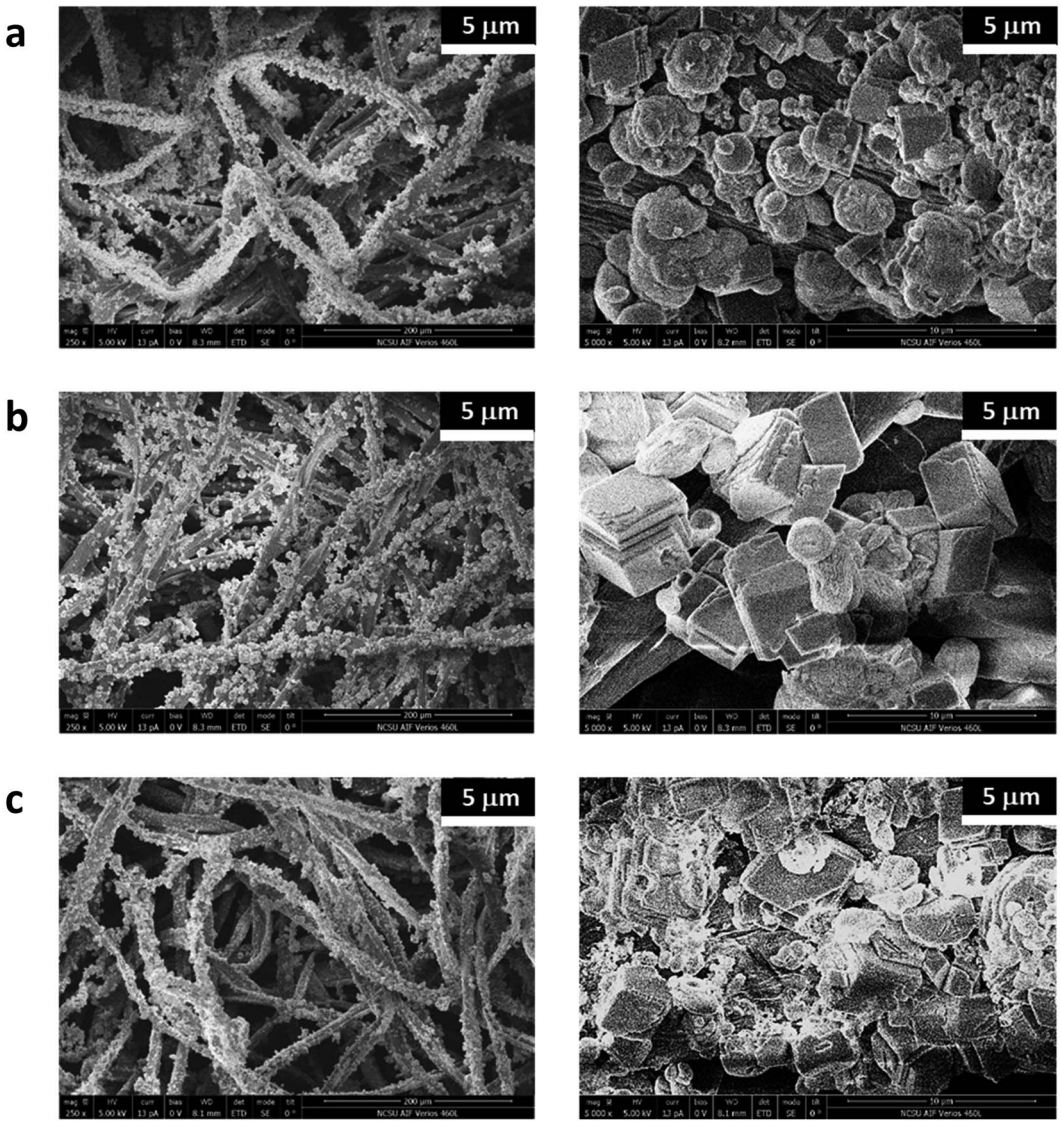

Fig. 4 SEM images of mineralized (a) raw, (b) scoured, and (c) brown cotton nonwoven fabrics taken with magnifications of 250× (left) and 5000× (right).

Fig. 3 shows the ATR-FTIR spectra of cotton nonwoven fabrics before and after mineralization. Control fabrics show characteristic bands for cotton cellulose: OH stretching (3600–3100 cm^{-1}), CH stretching (3000–2700 cm^{-1}), CH_2 bending (1428 cm^{-1}), COC stretching (1160 cm^{-1}), CO stretching (1053 and 1033 cm^{-1}), and glucose ring stretching (898 cm^{-1}). Non-cellulosic components for raw cottons did not show recognizable bands. The mineralization diminished the characteristic bands of cotton and intensified the characteristic bands of $CaCO_3$, indicating its coverage of the fiber surface. All mineralized cottons exhibited a strong band at 874 cm^{-1}, which are from the CO_3 out-of-plane bending of both calcite and vaterite polymorphs. The band at 713 cm^{-1} was attributed to the stretching of calcite.[35] The band at 744 cm^{-1}, which is a characteristic vibration band of vaterite,[35] appeared for all mineralized cottons but weakly appeared for m-Scoured. These results agree well with the XRD measurements.

Fig. 4 shows the SEM images of the mineralized cotton nonwoven fabrics at low and high magnifications. The low-magnification images show that $CaCO_3$ particles were uniformly grown on the surface of individual fibers of raw, scoured, and brown cottons. Under the high magnification, the morphological structures of the $CaCO_3$ particles were found to be distinctive for different cotton hosts. For raw cotton, a mixture of spherical and rhombic shaped particles was observed. Calcite, vaterite, and aragonite polymorphs have rhombus, spherulite, and needle-like shapes, respectively.[34] The coexistence of calcite and vaterite morphologies on raw cotton is in line with the earlier results of XRD, Raman spectroscopy, and ATR-FTIR spectroscopy. The size of vaterite crystallites was varied, and some of them were observed to be in aggregates. For scoured cotton, most particles were relatively well-defined rhombic, and their size was greater than that of the particles formed on raw cotton. For brown cotton, the structure of particles was less defined as compared with those on raw and scoured cotton fibers. Irregular particles were agglomerated to each other. The elemental compositions of the fabric surfaces were characterized using EDS (Fig. 5). The strong peaks of Ca element were observed in the energy spectra of all cotton samples. No appreciable peaks of contaminants, *i.e.*, Na and Cl, were observed. The EDS maps of Ca element demonstrate its uniform distribution over the fabric surfaces. It was observed that the Ca element was more densely occupied on the scoured cotton, being in line with the larger size and more well-defined morphology of calcite polymorph in the SEM image.

A combination of analyses indicate that cotton nonwoven fabrics having netlike architecture effectively hosted the formation of $CaCO_3$ polymorphs. Abundant electron-donating groups (*e.g.*, hydroxyl groups) on the surface of cotton fibers act as calcium binding sites during the dipping procedure in an aqueous $CaCl_2$ solution. The local supersaturation of Ca^{2+} on the fiber surface led to nucleation with HCO_3^- that was introduced by the subsequent dipping in an aqueous Na_2CO_3 solution. The nucleus further developed to form a crystal. The

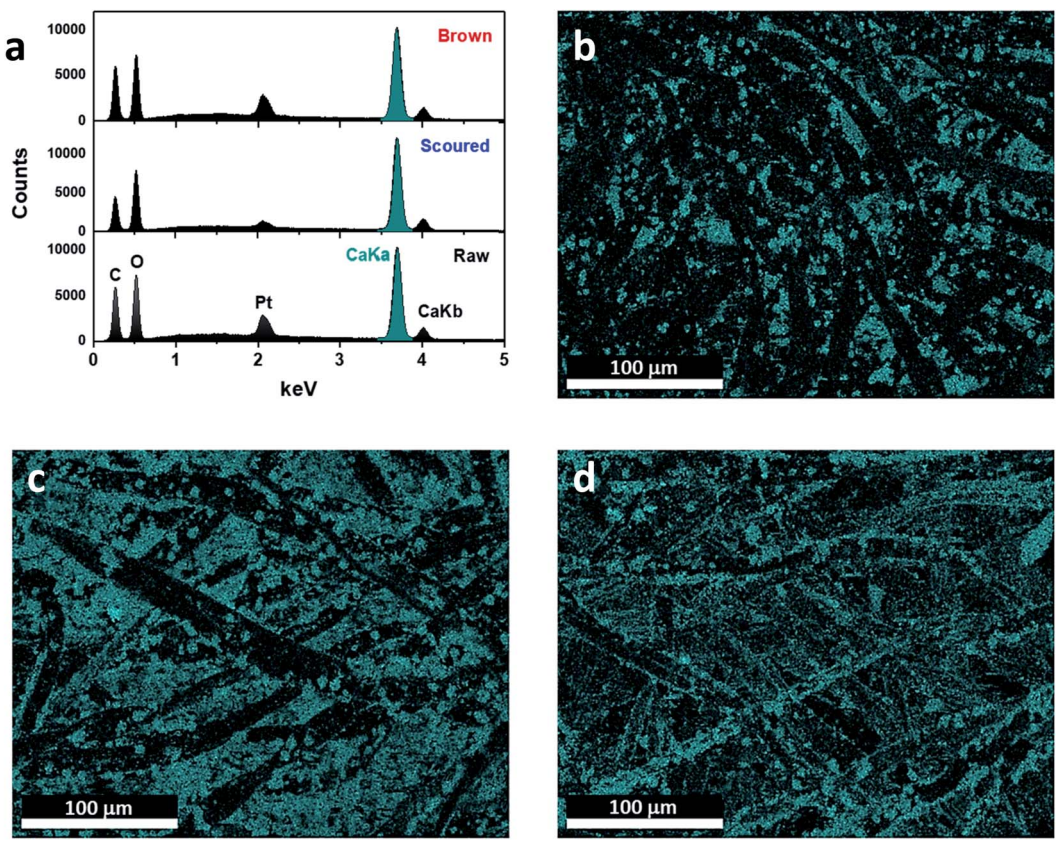

Fig. 5 EDS analysis: (a) spectra and maps of calcium element for the mineralized (b) raw, (c) scoured, and (d) brown cotton nonwoven fabrics.

surface chemistry of cotton varieties associated with naturally occurring components influenced the development of the crystal polymorph. The vaterite formation favored by raw and brown cottons was attributed to the presence of proteins on the fiber surface. It has been reported that proteins modify the growth of $CaCO_3$ crystals.[36–38] Depending on their chemistry and structure, proteins stabilized vaterite and delayed its transformation into calcite. Cotton, whose proteins were removed by scouring, promoted the formation of calcite.

3.2. Improvement of thermal resistance

The effects of the $CaCO_3$ mineralization on the thermal properties of cotton nonwoven fabrics were examined. Fig. 6 shows TG and DTG thermograms of raw, scoured, and brown fabrics before and after mineralization taken under nitrogen environment at a heating rate of 10 °C min^{-1}. Control cottons exhibited a typical three-stage weight loss: (1) loss of moisture at around 100 °C, (2) decomposition of cellulose at 320–380 °C and (3) decomposition of char above 380 °C. The decomposition of low-molecular-weight non-cellulosic components is likely to occur prior to the decomposition of high-molecular-weight cellulose. The greater weight loss in the initial stage (<320 °C) for brown cotton indicates the larger content of non-cellulosic components. However, brown cotton yielded a larger amount of char than raw and scoured cottons; 17.5% *vs.* 9.4 and 7.3%. The char yield is an important parameter in evaluating the thermal stability of materials because char can insulate the underlying substrate to protect from heat and prevent the release of combustible gases. The improved thermal stability of brown cotton was also demonstrated by its smaller DTG peak (Fig. 6c), which signifies less drastic thermal reactions of cellulose as compared with those of white cottons. This distinct thermal performance was associated with the presence of condensed tannins.[27] After mineralization, cottons showed a four-stage weight loss with the additional stage at 600–680 °C. This stage corresponded to the process of $CaCO_3$ decarbonation, which produces calcium oxide and carbon dioxide.[39] As carbon dioxide is lost to the atmosphere, this dissociation process is irreversible. When comparing the DTG peaks of the control cottons, the peaks of mineralized cottons were smaller, indicating that the thermal reactions of cellulose were less vigorous. The peak temperature for raw and scoured cottons shifted to a slightly higher temperature, whereas that for brown cotton shifted to a slightly lower temperature after mineralization. These results indicate that the mineralization influenced the thermal reactions of cellulose. The $CaCO_3$ coat, which decomposed at a temperature much higher than cellulose, potentially acted as a thermal barrier for cotton fibers.

The activation energy (E_a) for the thermal decomposition was determined by the isoconversional Friedman method.[23] Fig. 7a

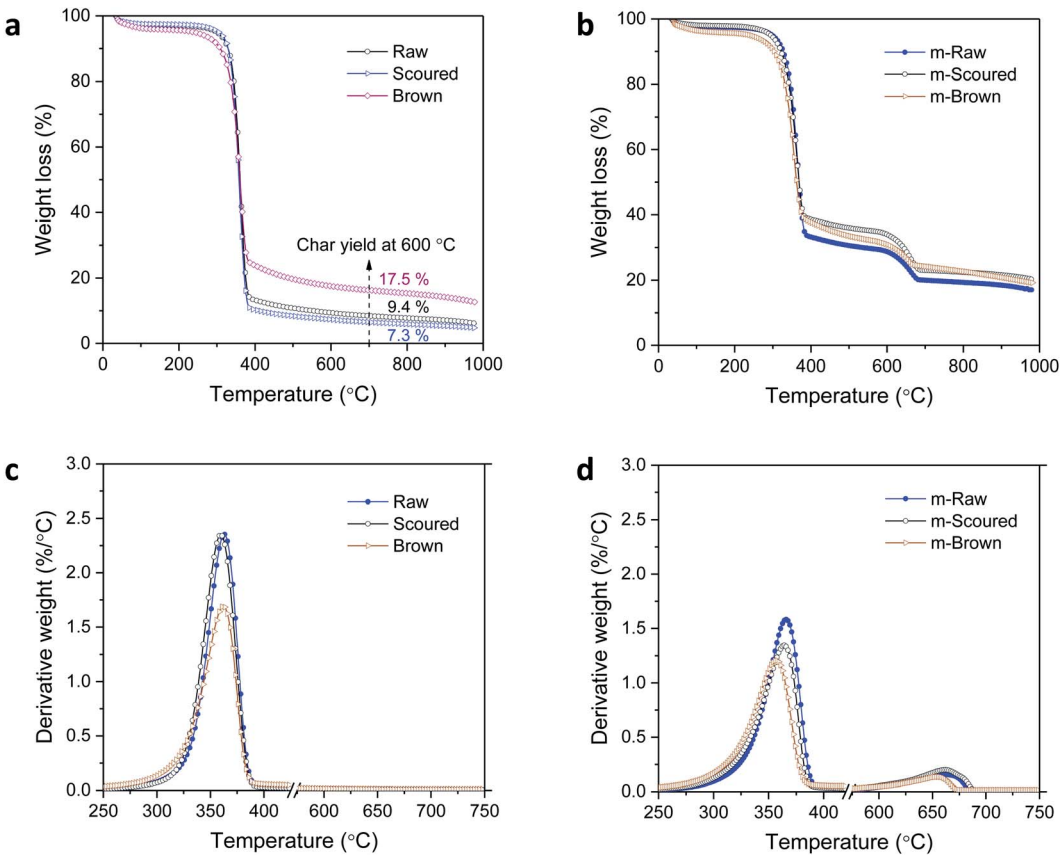

Fig. 6 TG thermograms of raw, scoured, and brown cotton nonwoven fabrics (a) before and (b) after mineralization taken under nitrogen environment at a heating rate of 10 °C min^{-1}. Their corresponding DTG thermograms (c) before and (d) after mineralization.

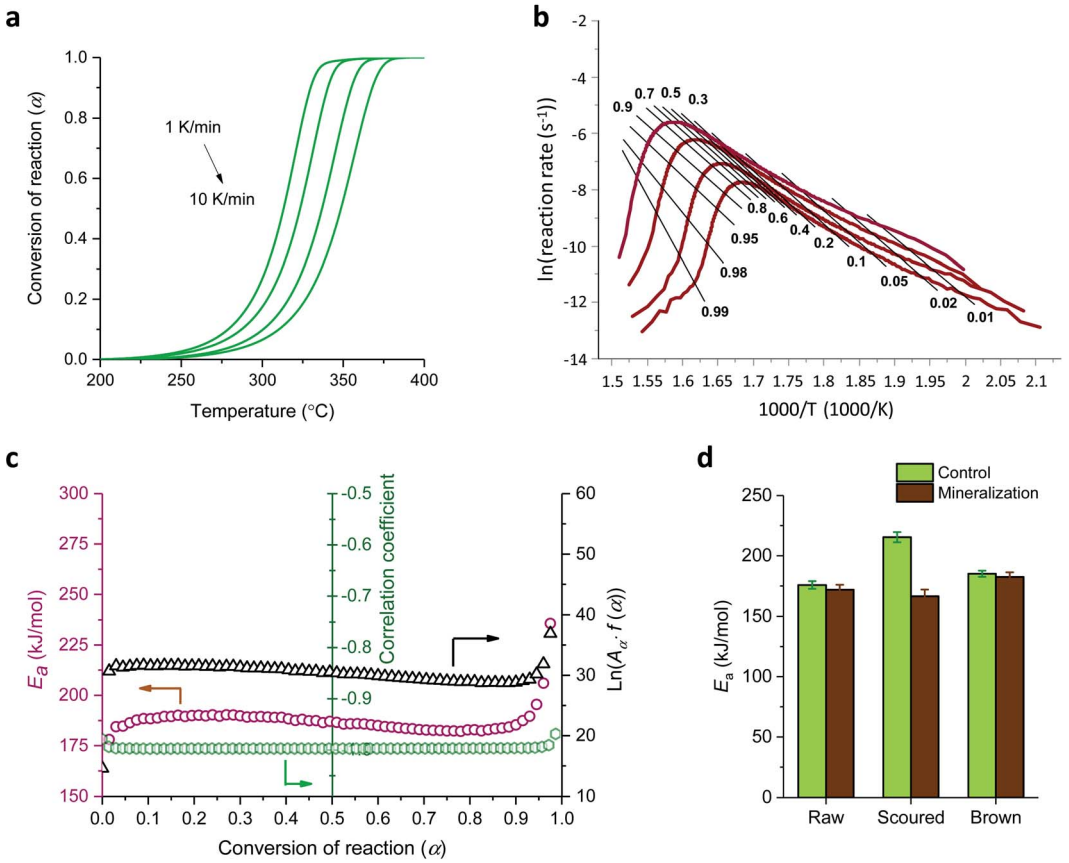

Fig. 7 Thermal kinetic analysis of mineralized brown cotton: (a) conversion of reaction as a function of temperature at four heating rates, (b) differential isoconversional analysis, and (c) activation energy, natural logarithm of the pre-exponential factor times the reaction model, and correlation coefficient as a function of the conversion of the reaction. (d) Activation energies for the thermal decomposition of cottons before and after mineralization.

shows a typical dependence of the conversion of reaction (α) on temperature for m-Brown cotton as an example. The thermal reaction decelerated when α was close to 0 and 1, and its rate reached the maximum at the intermediate extent of the conversion. As the heating rate increased, the α shifted toward a higher temperature. Fig. 7b shows the plots of the natural

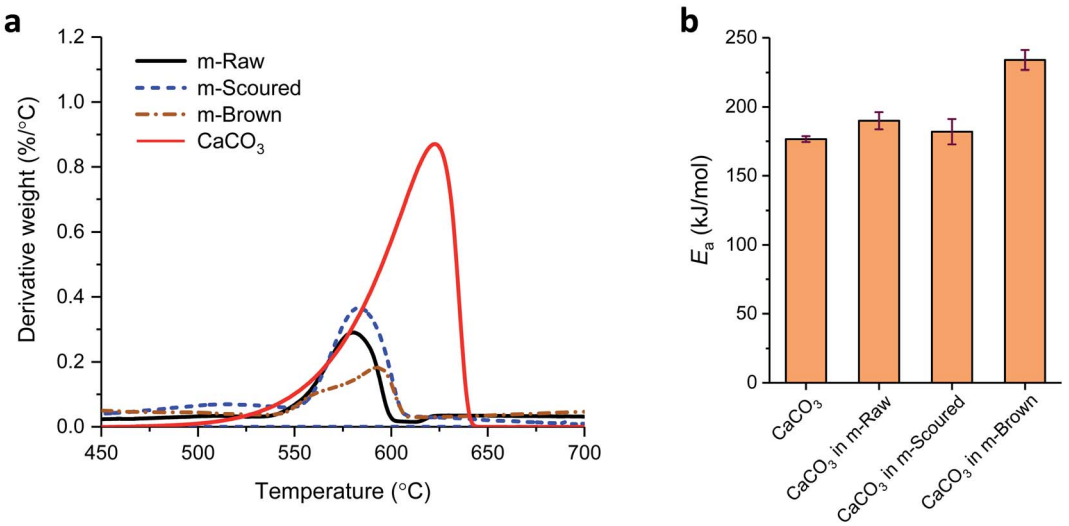

Fig. 8 (a) DTG thermograms of $CaCO_3$ polymorphs on raw, scoured, and brown cottons collected under nitrogen environment at a heating rate of 1 °C min^{-1}. (b) E_a values for the thermal decomposition of $CaCO_3$ formed on various cottons. The data of reagent-grade $CaCO_3$ are presented as well for comparison.

logarithm of reaction rate as a function of the reciprocal temperature at fifteen incremental α values. All plots have linear relationships, signifying the validity of the differential method. The analysis was conducted with a 0.0001 interval of α, and fifteen values were shown here. Using eqn (6), the E_a was calculated from the slope of the straight line $(-E_a(\alpha)/R)$. Fig. 7c shows the plot of E_a obtained for all α values. Except for the stages near $\alpha = 0$ or 1, E_a was relatively steady over the course of α for all samples. Similarly, the intercept of the straight line, $\ln(A(\alpha)f(\alpha))$, was independent of α. The correlation coefficients of the linear relationship were all greater than 0.99 for $\alpha = 0.1$–0.9. Fig. 7d shows the average values of E_a taken from $\alpha = 0.1$ to $\alpha = 0.9$ for cottons before and after mineralization. The E_a for scoured cotton was greater than those of raw and brown cottons, but the mineralization significantly lowered the E_a of the scoured cotton.

Fig. 8a and b show their DTG curves and E_a values, respectively, for the decarbonation of $CaCO_3$. The DTG peak temperatures for $CaCO_3$ on raw, scoured, and brown cottons were 580.4, 583.5, and 592.8 °C, respectively. These temperatures were lower than the peak temperature of 620.5 °C determined for reagent-grade $CaCO_3$. This difference was attributed to factors that influence the decarbonation temperature such as grain size, intergranular texture, and impurities.[40] The irregular grains on brown cotton observed in the SEM image (Fig. 4c) might be responsible for a broader peak with a shoulder at a low temperature. By selecting these DTG peaks at different heating rates, the E_a for the decarbonation was determined (Fig. 8b). The E_a for reagent-grade $CaCO_3$ was 177 kJ mol^{-1}, which is close to the value (167 kJ mol^{-1}) determined using the Ozawa–Flynn–Wall method in other study.[39] Compared with this value, a noticeable increase in E_a was observed for $CaCO_3$ formed on brown cotton.

MCC simulates combustion by pyrolyzing a sample at a constant heating rate and subsequently oxidizing the released gases to provide heat release parameters. As MCC parameters have good correlations with conventional flammability test values,[41–43] they are useful in predicting the flammability of materials. Table 1 presents MCC parameters including HRC, PHRR, TPHRR, THR, and char yield for raw, scoured, and brown cotton nonwovens before and after mineralization. Before mineralization, the superior thermal stability of brown cotton was demonstrated by its lower HRC, PHRR, TPHRR, and THR as well as greater char yield as compared with those of raw and

Table 1 Microscale combustion calorimetric (MCC) data for raw, scoured, and brown cotton nonwoven fabrics before and after mineralization

		HRC (J g^{-1} K^{-1})	PHRR (W g^{-1})	TPHRR (°C)	THR (kJ g^{-1})	Char yield (%)
Raw	Control	284.5 (4.5)[a]	332.7 (3.8)	374.3 (2.1)	13.2 (0.7)	8.5 (0.8)
	Mineralized	215.0 (9.0)	253.1 (9.6)	389.7 (5.6)	9.5 (1.2)	26.6 (1.5)
Scoured	Control	302.0 (5.5)	335.0 (5.3)	390.4 (2.8)	14.5 (0.9)	6.0 (1.1)
	Mineralized	183.0 (7.6)	215.2 (5.9)	389.7 (4.3)	8.8 (1.2)	29.6 (2.3)
Brown	Control	191.3 (4.1)	229.3 (3.9)	387.7 (3.2)	8.9 (1.1)	19.6 (1.2)
	Mineralized	125.7 (8.2)	150.6 (6.1)	384.4 (4.8)	6.5 (2.1)	34.6 (3.6)

[a] Standard deviation of three measurements.

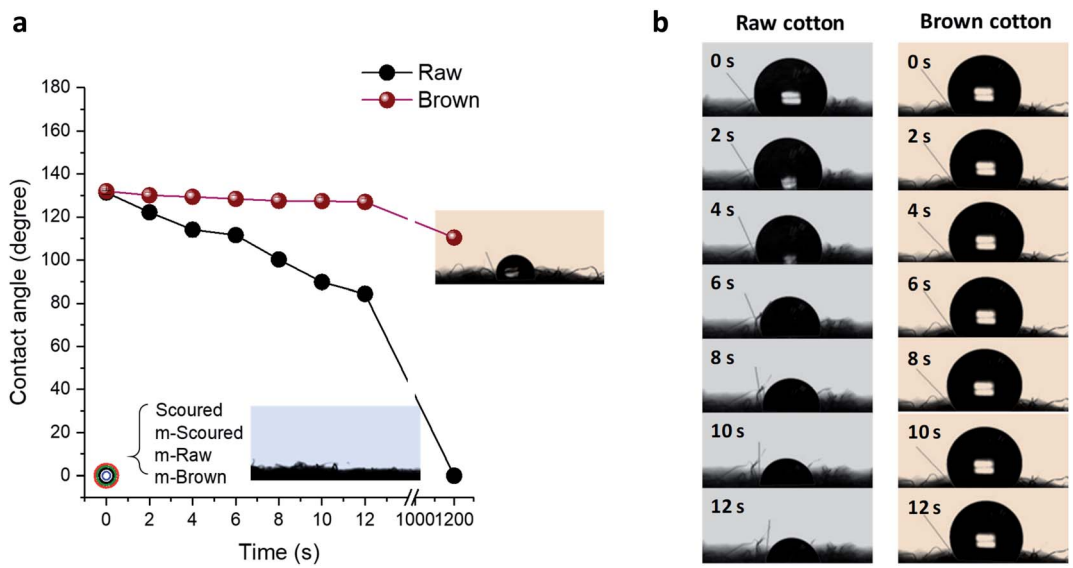

Fig. 9 (a) Contact angles of water droplets on the nonwoven fabrics as a function of time. The error bars are smaller than the size of symbols. (b) Time lapse photographs of water droplets on the nonwoven fabrics.

scoured cottons. After mineralization, the HRC values of all cottons were significantly reduced. In particular, the scoured cotton exhibited the largest reduction in HRC by about 40%.

3.3. Alteration of surface property

Raw white and brown cotton nonwoven fabrics are hydrophobic because of the presence of waxes and pectin on the fiber surface. As can be seen in Fig. 9, the contact angles of a water droplet on the raw white and brown fabrics, which were measured immediately after drop deposition, were about 130 degrees. Surfaces with a contact angle greater than 90 degrees are considered as hydrophobic. The scoured cotton fabric immediately absorbed the water droplet (recorded as zero degree). As the time increased to 12 seconds, the contact angle for raw cotton gradually decreased to about 84 degrees, whereas the contact angle for brown cotton remained unchanged. These distinctive behaviors were attributed to different area densities of nonwoven fabrics, *i.e.*, 55 g m^{-2} and 127 g m^{-2} for raw white and brown fabrics, respectively. For the low-density fabric, the water droplet spread *via* wicking through the voids in the loosely hydroentangled structure. For high-density fabric, the contact angle was greater than 90 degrees until the water droplet was dried. *i.e.*, 110 degrees after 20 min, in which the water droplet was dried and shrunken (inset of Fig. 9a). After mineralization of these fabrics, the water droplet immediately spread onto the fabric, so any visible contact angles were not be able to be measured. These results show that the mineralization of raw white and brown cottons can transform the nature of their surfaces from hydrophobic to hydrophilic similar to that of scoured cotton.

The effect of $CaCO_3$ mineralization on the moisture absorption properties of various cotton nonwoven fabrics was examined. Fig. 10 shows the percentage of moisture regains for raw, scoured, and brown cottons before and after mineralization as a function of conditioning time at 40 °C and 90% RH. The initial moisture regain of scoured cotton was greater than those of raw and brown cottons, *i.e.*, 1.5%, 2.2%, and 1.8% at 5 min for raw, scoured, and brown cottons, respectively. In comparison of raw cottons, brown cotton exhibited slightly higher moisture regains than white cotton. This was in line with the results from other study, in which the water contents of raw white and raw brown cotton were determined to be 6.82% and 7.88%, respectively, using the Karl Fischer titration reference method.[44] The moisture regains for all cottons rapidly increased within 10 min, beyond which no further increases were observed. After mineralization, the moisture regain greatly increased for all cottons. The mineralized raw and scoured cottons absorbed moisture about twice than the respective control cottons. The moisture regains of mineralized scoured and brown cotton levelled off at 10 min, whereas that of mineralized raw cotton levelled off at 30 min. The improved moisture regain was attributed to the hydration of $CaCO_3$ surfaces. It has been reported that the surface of $CaCO_3$ lattice planes is readily hydrated as the oxygen atoms of the water molecules are coordinated with the surface calcium ions or by hydrogen bonding to a surface oxygen.[45] Such adsorption of

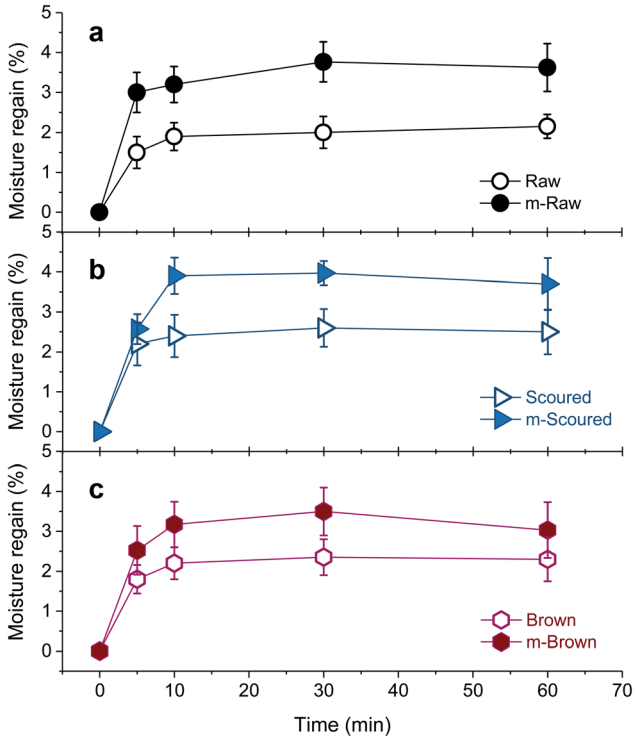

Fig. 10 Percentage moisture regains of (a) raw, (b) scoured, and (c) brown cotton nonwoven fabrics before and after mineralization measured at 40 °C and 90% RH.

a monolayer of water stabilizes all calcite and vaterite surfaces.[45] Our observations suggest that the polymorph selection is not crucial in improving the water- and moisture-absorption properties of cottons.

4. Conclusions

A majority of cotton products on the market are made of scoured and/or bleached white fibers. Since scouring and bleaching processes that remove non-cellulosic materials (waxes, proteins, pectin, and natural pigment) cause high chemical and biological oxygen demands in the textile effluents,[46] the use of raw white or raw colored cotton fibers is receiving growing attention.[47] In this study, cotton varieties including raw (unscoured and unbleached) white and brown cottons were investigated as host materials for the growth of $CaCO_3$ polymorphs to improve and alter their properties for nonwoven applications. The mineralization method employed was a simple process of cyclic dipping, which introduces calcium and carbonate ions to cottons in alternation. A combination of analyses using XRD, Raman spectroscopy, ATR-FTIR spectroscopy, SEM, and EDS agreed that hydroentangled cotton nonwoven fabrics were successfully mineralized without seeding. The surface chemistry of the fibers affected the polymorphism of $CaCO_3$. Scoured cotton fabric predominantly produced the most stable polymorph, calcite, while raw white and raw brown cottons promoted the formation of partial vaterite phase. The proteins present on raw cottons were

considered to stabilize the metastable polymorph of vaterite, delaying the polymorphic transformation. The $CaCO_3$ mineralization altered the hydrophobic surface of raw cotton nonwovens, which yielded about 130 degrees of a water contact angle, into the hydrophilic surfaces, which immediately absorbed the water droplet. The moisture regains of mineralized cottons including scoured cotton were increased by nearly double as compared with those of control cottons. Furthermore, the mineralized cotton nonwovens exhibited improved thermal resistance. Their heat release capacity, which is associated with flammability, decreased up to 40% after mineralization. The thermal decomposition of cotton cellulose insulated with $CaCO_3$ polymorphs became slower, and its activation energy was decreased. This study extends the understanding for the opportunity of biomineralization to cotton materials and provides a new possible route for expanding the application of raw white and colored cotton nonwovens.

Conflicts of interest

There are no conflicts of interest to declare.

Acknowledgements

The authors are grateful to the ARS Innovation Fund to support the internship of N. Ernst.

References

1 H. A. Lowenstam and S. Weiner, *On Biomineralization*, Oxford University Press, New York, 1989.
2 N. Watabe, *J. Cryst. Growth*, 1974, **24/25**, 116–122.
3 N. A. Sommerdijk and G. de With, *Chem. Rev.*, 2008, **108**, 4499–4550.
4 T. Kokubo, *J. Non-Cryst. Solids*, 1990, **120**, 138–151.
5 G. J. Liu, F. Miyaji, T. Kokubo, H. Takadama, T. Nakamura and A. Murakami, *J. Mater. Sci.: Mater. Med.*, 1998, **9**, 285–290.
6 T. Tetsushi, K. Akio and A. Mitsuru, *Chem. Lett.*, 1988, **27**, 711–712.
7 D. Yang, K. Yu, Y. Ai, H. Zhen, J. Nie and J. F. Kennedy, *Carbohydr. Polym.*, 2011, **84**, 990–996.
8 A. Suslu, A. Z. Albayrak, A. S. Urkmez, E. Bayir and U. Cocen, *J. Mater. Sci.: Mater. Med.*, 2014, **25**, 2677–2689.
9 X. N. Chen, L. S. Wan, Q. Y. Wu, S. H. Zhi and Z. K. Xu, *J. Membr. Sci.*, 2013, **441**, 112–119.
10 S. H. Zhi, L. S. Wan and Z. K. Xu, *J. Membr. Sci.*, 2014, **454**, 144–154.
11 Y. Park, P. Rawat and E. Ford, *Ind. Eng. Chem. Res.*, 2017, **56**, 8241–8250.
12 E. Dalas, J. Kallitsis and P. G. Koutsoukos, *J. Cryst. Growth*, 1988, **89**, 287–294.
13 H. Konno, Y. Nanri and M. Kitamura, *Powder Technol.*, 2002, **123**, 33–39.
14 M. Kitamura, H. Konno, A. Yasui and H. Masuoka, *J. Cryst. Growth*, 2002, **236**, 323–332.
15 Z. Hu and Y. Deng, *Powder Technol.*, 2004, **140**, 10–16.
16 J. W. Ahn, J. H. Kim, H. S. Park, J. A. Kim, C. Han and H. Kim, *Korean J. Chem. Eng.*, 2005, **22**, 852–856.
17 Y. Shinya, O. Takahiro, K. Yuya, A. Hiroya, H. Kenji, F. Toshiyuki and K. Yoshikazu, *J. Nanopart. Res.*, 2014, **16**, 2266.
18 P. J. Wakelyn, N. R. Bertoniere, A. D. French, D. P. Thibodeaux, B. A. Triplett, M. Rousselle, W. R. Goynes Jr, J. V. Edwards, L. Hunter, D. D. McAlister and G. R. Gamble, *Cotton Fiber Chemistry and Technology*, CRC Press, Boca Raton, 2006.
19 S. Hua, X. Wang, S. Yuan, M. Shao, X. Zhao, S. Zhu and L. Jiang, *Crop Sci.*, 2007, **47**, 1540–1546.
20 T. Li, H. Fan, Z. Li, J. Wei, Y. Lin and Y. Cai, *Acta Physiol. Plant.*, 2012, **34**, 813–818.
21 A. P. S. Sawhney, B. Condon, M. Reynolds, R. Slopek and D. Hui, *Text. Res. J.*, 2010, **80**, 1540–1549.
22 A. P. S. Sawhney, M. Reynolds, B. Condon, R. Slopek and C. Allen, *Text. Res. J.*, 2011, **81**, 1484–1492.
23 H. L. Friedman, *J. Polym. Sci., Part C: Polym. Symp.*, 1964, **6**, 183–195.
24 G.-T. Zhou, J. C. Yu, X.-C. Wang and L.-Z. Zhang, *New J. Chem.*, 2004, **28**, 1027.
25 W.-S. Kim, I. Hirasawa and W.-S. Kim, *Ind. Eng. Chem. Res.*, 2004, **43**, 2650–2657.
26 H. G. M. Edwards, D. W. Farwell and A. C. Williams, *Spectrochim. Acta, Part A*, 1994, **50**, 807–811.
27 S. Nam, H. J. Kim, B. D. Condon, D. J. Hinchliffe, S. Chang, S. C. McCarty and C. A. Madison, *Cellulose*, 2016, **23**, 1137–1152.
28 Z. Pan, D. Sun, J. Sun, Z. Zhou, Y. Jia, B. Pang, Z. Ma and X. Du, *Euphytica*, 2010, **173**, 141–149.
29 L. Zhang, H. Jianxin and S. Y. Wang, *J. Therm. Anal. Calorim.*, 2009, **95**, 653–659.
30 Y. H. Xiao, Z. S. Zhang, M. H. Yin, M. Luo, X. B. Li, L. Hou and Y. Pei, *Biochem. Biophys. Res. Commun.*, 2007, **358**, 73–78.
31 Z. Zou, L. Bertinetti, Y. Politi, A. C. S. Jensen, S. Weiner, L. Addadi, P. Fratzl and W. J. E. M. Habraken, *Chem. Mater.*, 2015, **27**, 4237–4246.
32 Z. Zheng, B. Huang, H. Ma, X. Zhang, M. Liu, Z. Liu, K. W. Wong and W. M. Lau, *Cryst. Growth Des.*, 2007, **7**, 1912–1917.
33 S. Xu, Z. Ye and P. Wu, *ACS Sustainable Chem. Eng.*, 2015, **3**, 1810–1818.
34 A. Dandeu, B. Humbert, C. Carteret, H. Muhr, E. Plasari and J. M. Bossoutrot, *Chem. Eng. Technol.*, 2006, **29**, 221–225.
35 M. Ni and B. D. Ratner, *Surf. Interface Anal.*, 2008, **40**, 1356–1361.
36 A. W. Xu, Y. Ma and H. Cölfen, *J. Mater. Chem.*, 2007, **17**, 415–449.
37 V. P. Shastri, *MRS Bull.*, 2015, **40**, 473–477.
38 M. Sarem and S. Lüdeke, *MRS Bull.*, 2015, **40**, 490–498.
39 V. Georgieva, L. Vlaev and K. Gyurova, *J. Chem.*, 2013, **2013**, 872981.
40 G. T. Faust, *Am. Mineral.*, 1950, **38**, 207–224.
41 R. E. Lyon, R. N. Walters and S. I. Stoliarov, *Polym. Eng. Sci.*, 2007, **47**, 1501–1510.

42 C. Q. Yang, Q. He, R. E. Lyon and Y. Hu, *Polym. Degrad. Stab.*, 2010, **95**, 108–115.
43 C. Q. Yang and Q. L. He, *Fire Mater.*, 2012, **36**, 127–137.
44 J. Montalvo, T. V. Hoven, M. Easson and D. Hinchliffe, *AATCC J. Res.*, 2016, **3**, 12–26.
45 N. H. de Leeuw and S. C. Parker, *J. Phys. Chem. B*, 1998, **102**, 2914–2922.
46 H. L. Chen and L. D. Burns, *Cloth. Text. Res. J.*, 2006, **24**, 248–261.
47 S. Levy, *Meet Fibers' Green Dream Team*, https://www.nonwovens-industry.com/issues/2010-06/view_features/meet-fibers-green-dream-team/, accessed 8/2020.